Available online at www.sciencedirect.com

ScienceDirect

IFAC PapersOnLine 56-2 (2023) 4466–4471

Distributed Regulation of the Safety Factor Profile in Tokamaks Using Nonlinear Infinite-dimensional Control ⋆

Sai Tej Paruchuri * **Eugenio Schuster** *

* *Mechanical Engineering and Mechanics, Lehigh University, Bethlehem, Pennsylvania, USA (e-mail: saitejp@lehigh.edu).*

Abstract: Tokamaks are toroidal devices that use helical magnetic fields to confine a plasma (hot ionized gas). Such confinement increases the probability of ionic collisions. When the colliding ions have high enough kinetic energy, they can overcome the Coulombic forces of repulsion and fuse to form a heavier ion. The difference in mass between reactant and product ions is turned into energy, which can potentially be harvested to meet the growing world's energy demands. In tokamaks, the safety factor profile is a plasma property that characterizes the pitch of the helical magnetic field. Experiments have shown that the safety factor is related to the magnetohydrodynamic (MHD) stability of the confined plasma as well as to the capability of achieving highly-confined steady-state operation. Thus, active control of the safety factor profile or related plasma properties is critical for achieving MHD-stable, high-performance plasma operation. The evolution of the safety factor profile is governed by a nonlinear nonautonomous partial differential equation (PDE). The most commonly used control design approach reduces the governing PDE to a set of ordinary differential equations (ODEs) before synthesizing a control law. In this work, a distributed nonlinear safety-factor control law that does not require a finite-dimensional approximation of the governing PDE is proposed. Rigorous analysis shows that the proposed control law can drive the error between the safety factor profile and target profile to zero. The effectiveness of the proposed control law is demonstrated using nonlinear simulations for the DIII-D tokamak.

Keywords: Plasma Control, Partial Differential Equation, Safety Factor Control, Distributed Control, Nonlinear Control, Nuclear Fusion.

1. INTRODUCTION

Nuclear fusion has been proposed as one of the potential solutions to meet the world's growing energy needs in the forthcoming decades. In nuclear fusion, two or more nuclei combine to form a heavier nucleus. The difference in mass between the reactants and the products is released as energy. Only those positively-charged nuclei with high enough kinetic energy to overcome the Coulombic forces of repulsion can undergo nuclear fusion when they collide. Thus, maintaining high temperatures (around 10^8 K) and consequently a high probability of collisions among the reactants are critical, among other factors, to achieving nuclear fusion. Different configurations have been proposed as potential solutions for realizing nuclear fusion. Of these, *tokamaks* are the most developed and researched devices (Wesson and Campbell, 2011). Tokamaks are torus-shaped devices that use magnetic fields to confine a plasma (a hot ionized gas). Such confinement is possible since the plasma exists in the form of positively-charged ions and negatively-charged electrons, which react to external magnetic fields.

The *safety factor* is a plasma parameter that characterizes the pitch of the helical magnetic field lines in a tokamak. The spatial variation of the safety factor from the magnetic axis to the plasma edge (refer to Figure 1) defines the *safety factor profile*. Magnetohydrodynamic (MHD) studies show that the safety factor profile is related to the stability of the confined plasma, and achieving stable confinement in a tokamak requires maintaining the profile at preset levels. For instance, MHD instabilities like neoclassical tearing modes (NTMs) can appear at locations where the safety factor is a rational value (Wesson and Campbell, 2011). Fusion reactors must also operate in scenarios characterized by a high bootstrap current (self-generated current produced due to pressure gradients in the tokamak) to achieve steady-state conditions. Maintaining the safety factor profile at optimal levels is critical to achieving scenarios characterized by high bootstrap current. Due to the presence of external disturbances, active control algorithms are required to regulate plasma parameters like the safety factor profile.

Safety-factor-control algorithms in the literature can be broadly classified into local and global control algorithms. Local control algorithms are designed to regulate the scalar safety factor values at specific locations, i.e., safety factor at the core q_0 (Boyer et al., 2015), safety factor minimum

⋆ This material is based upon work supported by the U.S. Department of Energy, Office of Science, Office of Fusion Energy Sciences, under Award Numbers DE-SC0010537 and DE-SC0010661.

10.1016/j.ifacol.2023.10.934

q_{min} control (Paruchuri et al., 2021). On the other hand, the objective of global control is to regulate the whole safety factor profile. Solutions for global safety factor control have been developed based on optimal control (Wehner et al., 2017), predictive control (Ou et al., 2011), robust control (Barton et al., 2015), feedback linearization (Pajares and Schuster, 2016). Safety factor dynamics is modeled using a nonlinear nonautonomous partial differential equation. The above-cited control algorithms rely on the *approximate-then-design* (ATG) approach, where the model is reduced to an ordinary differential equation (ODE) before synthesizing the "finite-dimensional" controller. The performance of the finite-dimensional controller, when implemented to regulate the original infinite-dimensional plant, depends on the model approximation scheme used and can be hard to quantify mathematically. On the other hand, the *design-then-approximate* (DTA) approach, which synthesizes an infinite-dimensional controller based on the distributed parameter model and then introduces an approximation to obtain a finite-dimensional controller that is useful for practical implementation, provides a comparatively easier way to quantify the effect of approximation error on closed-loop performance. However, a controller based on the DTA approach is much more complex to synthesize in most practical scenarios due to the infinite-dimensional nature of the underlying control problem. Nevertheless, linear control algorithms based on the DTA approach have been developed and successfully implemented for safety factor regulation in tokamaks (Argomedo et al., 2013a,b; Mavkov et al., 2018).

As mentioned, advanced scenarios associated with next-generation tokamaks rely on a high bootstrap-current fraction. The effect of the bootstrap current on the safety factor dynamics is nonlinear. Thus, a linear approximation of the bootstrap current contributions to the plasma dynamics may not always be sufficient in such high bootstrap current scenarios. This work develops a nonlinear distributed Lyapunov-based control algorithm that can drive the safety factor profile to the desired target. The underlying dynamics model used for synthesizing the control law accounts for the nonlinear effects of the bootstrap current. A rigorous analysis is presented to show that the controller can stabilize the error system. The infinite-dimensional control law is then approximated using a finite-difference scheme. Such approximation enables the computation of actual physical inputs (powers of current drives set for safety factor control) from the virtual input (controller demand computed from the infinite-dimensional control law). The effect of model uncertainties and approximation errors on the closed-loop system's performance is also discussed in detail. The proposed controller is shown to be effective in a DIII-D tokamak scenario using nonlinear simulations.

This paper is organized as follows. Section 2 develops the distributed-parameter model for poloidal flux gradient (a parameter related to the safety factor). This model is used in Section 3 to synthesize the infinite-dimensional controller. The control law approximation is also presented in Section 3. Section 4 presents the results of simulation studies carried out to test the effectiveness of the proposed control law. Finally, Section 5 concludes the paper and discusses potential future extensions of this work.

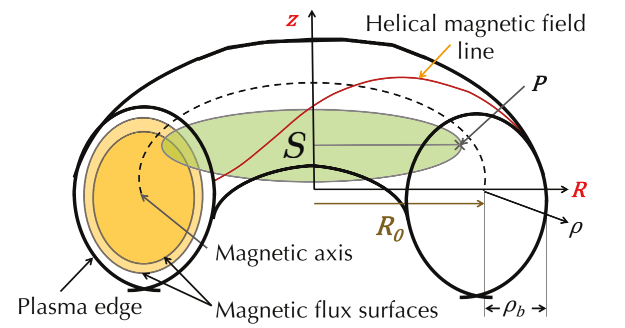

Fig. 1. Magnetic field lines and flux surfaces in a tokamak.

2. DISTRIBUTED PARAMETER MODEL

2.1 Preliminary Definitions

The helical magnetic field lines in the tokamak can be decomposed into the poloidal magnetic field $\bar{B}_\theta$ and the toroidal magnetic field $\bar{B}_\phi$. The poloidal magnetic flux Ψ at a point P in the tokamak is defined as $\Psi := \int_S \bar{B}_\theta \cdot d\bar{S}$, where S is the surface enclosed by the loop contained in the horizontal plane and passing through the point P (refer to Figure 1). Under ideal MHD conditions, regions of constant magnetic flux form nested flux surfaces as shown in Figure 1. The safety factor q (defined below) takes a constant value on these flux surfaces. As a result of constant q values on flux surfaces and axisymmetry of tokamaks, a parameter that indexes the flux surfaces can be used as the spatial variable to model the safety factor dynamics. In this work, the normalized mean effectiveness minor radius $\hat{\rho}$ is used as the spatial variable. It is defined as $\hat{\rho} := \rho/\rho_b$, where ρ is the mean effectiveness minor radius that is given by $\rho := \sqrt{\Phi/B_{\phi,0}\pi}$. Here, the term Φ is the toroidal magnetic flux, and $B_{\phi,0}$ is the vacuum toroidal magnetic field at the major radius R_0 of the tokamak. Thus, the spatial variable $\hat{\rho}$ is obtained by normalizing ρ with its value at the last closed magnetic flux surface ρ_b. The safety factor at location $\hat{\rho}$ and time t is defined as

$$q(\hat{\rho}, t) := -\frac{d\Phi}{d\Psi} = -\frac{\partial\Phi/\partial\hat{\rho}}{\partial\Psi/\partial\hat{\rho}} = -\frac{B_{\phi,0}\rho_b^2\hat{\rho}}{\partial\psi/\partial\hat{\rho}}, \quad (1)$$

where $\psi = \Psi/2\pi$. The variation of the safety factor with $\hat{\rho}$ generates the "safety factor profile." Note that the safety factor is related to the poloidal flux gradient $\theta(\hat{\rho}, t) := \partial\psi(\hat{\rho}, t)/\partial\hat{\rho}$. Thus, the control of the poloidal flux gradient is equivalent to the regulation of the safety factor profile.

2.2 Poloidal Flux Gradient Model

The evolution of the poloidal stream function $\psi : (\hat{\rho}, t) \mapsto \psi(\hat{\rho}, t)$ is governed by the magnetic diffusion equation (MDE) (Hinton and Hazeltine, 1976), which is given by

$$\dot{\psi} = F(\hat{\rho})\left[G(\hat{\rho})\psi'\right]' + H(\hat{\rho})j_{ni}. \quad (2)$$

subject to the Neumann boundary conditions $\psi'|_{\hat{\rho}=0} = 0$, $\psi'|_{\hat{\rho}=1} = -k_{I_p}I_p$, where $F(\hat{\rho}) := \eta/(\mu_0\rho_b^2\hat{F}^2\hat{\rho})$, $G(\hat{\rho}) := \hat{\rho}\hat{F}\hat{G}\hat{H}$, $H(\hat{\rho}) := R_0\hat{H}\eta$, $(\cdot)' := \partial(\cdot)/\partial\hat{\rho}$, $\dot{(\cdot)} := \partial(\cdot)/\partial t$, In the above equations, the terms η, μ_0, j_{ni} and I_p are the plasma resistivity, vacuum permeability, noninductive current source and plasma current, respectively. It is assumed in this work that the plasma resistivity is estimated in real-time. The value of η is a function of the electron temperature T_e, which can indeed be estimated in real time as proposed in Morosohk et al. (2022). The terms $\hat{F}$, $\hat{G}$, $\hat{H}$ are geometric factors that depend on the plasma MHD equilibrium and are functions of the spatial variable $\hat{\rho}$. The term k_{I_p} in the boundary condition is a scalar constant, which is also a function of the MHD equilibrium.

The current driven in tokamaks can be decomposed into inductive and noninductive currents depending on their sources. Inductive currents are generated by a transformer-like effect where the magnetic coils in the tokamaks act as the primary coils and the plasma acts as the secondary coil. All the other current terms fall under the noninductive currents category. These includes the current driven by auxiliary drives such as neutral beam injectors (NBIs) and electron cyclotron heating and current drives (EC H&CDs) and the self-generated bootstrap current. Thus, the non-inductive current source j_{ni} is equal to the sum of the auxiliary current j_{aux} and bootstrap current j_{bs} sources, i.e., $j_{ni} = j_{aux} + j_{bs}$. In this work, the auxiliary current sources are considered the controllable inputs, i.e., the control law prescribes the auxiliary profile $j_{aux}(\cdot, t)$ at each time t. On the other hand, the bootstrap current source j_{bs} is determined by the control-oriented model used in Barton et al. (2013), which combines Sauter model (Sauter et al., 1999) with control oriented models for electron temperature and electron density. Note that the formula in Barton et al. (2013) assumes tight electron-ion coupling, i.e. $n_e = n_i$, $T_e = T_i$, where n_e, n_i are the electron and ion densities, respectively, and T_e, T_i are the electron and ion temperatures, respectively. The control-oriented model takes the form

$$j_{bs}(\hat{\rho}, t) = \underbrace{K_{bs} u_{bs}}_{L(\hat{\rho},t)} \frac{1}{\theta}, \tag{3}$$

where K_{bs} is a function of the spatial variable $\hat{\rho}$ and models the spatial distribution of bootstrap current. On the other hand, the term u_{bs} is a scalar that varies with time. It is defined as

$$u_{bs} := (I_p^{\gamma} P_{tot}^{\epsilon} \bar{n}_e^{\zeta})^{-1/2} \bar{n}_e, \tag{4}$$

where P_{tot} is the total plasma current, $\bar{n}_e$ is the line-averaged electron density, and γ, ϵ, ζ are scaling constants. In this work, the terms P_{tot}, $\bar{n}_e$ and I_p are assumed to be prescribed inputs.

Substituting the above model for bootstrap current (3) into the MDE (2) and taking the derivative on both sides with respect to the spatial variable $\hat{\rho}$ results in the partial differential equation

$$\dot{\theta} = \left[F\left[G\theta\right]'\right]' + \left[H j_{aux}\right]' + h_{bs}, \tag{5}$$

subject to the boundary conditions

$$\theta|_{\hat{\rho}=0} = 0, \qquad \theta|_{\hat{\rho}=1} = -k_{I_p} I_p, \tag{6}$$

where $h_{bs}(\hat{\rho}, \theta, \theta', t) = [H(\hat{\rho})L(\hat{\rho}, t)]' \frac{1}{\theta} - [H(\hat{\rho})L(\hat{\rho}, t)] \frac{\theta'}{\theta^2}$.

2.3 Error Model

Suppose that $\bar{\theta}$ is the target profile generated by $\bar{j}_{aux}$. Note that if a target safety factor profile $\bar{q}$ is given, the corresponding target poloidal flux gradient $\bar{\theta}$ can be computed from (1). Thus, the target poloidal flux gradient $\bar{\theta}$ satisfies the partial differential equation

$$\dot{\bar{\theta}} = \left[F\left[\ G\bar{\theta}\ \right]'\right]' + [H\bar{j}_{aux}]' + h_{bs}. \tag{7}$$

subject to the boundary conditions

$$\bar{\theta}\big|_{\hat{\rho}=0} = 0, \qquad \bar{\theta}\big|_{\hat{\rho}=1} = -k_{I_p} I_p. \tag{8}$$

Define the error state as $\tilde{\theta} := \theta - \bar{\theta}$. Subtracting (7) and (8) from (5) and (6) results in the error model of the form

$$\dot{\tilde{\theta}} = \left[F\left[G\tilde{\theta}\right]'\right]' + \left[H\tilde{j}_{aux}\right]' + \underbrace{h_{bs}(\hat{\rho}, \theta, \theta', t) - h_{bs}(\hat{\rho}, \bar{\theta}, \bar{\theta}', t)}_{\text{A}}, \tag{9}$$

subject to the boundary conditions

$$\tilde{\theta}\Big|_{\hat{\rho}=0} = 0, \qquad \tilde{\theta}\Big|_{\hat{\rho}=1} = 0, \tag{10}$$

where $\tilde{j}_{aux} = j_{aux} - \bar{j}_{aux}$. Before proceeding to control synthesis, it is critical to express Term A in (9) as a function of the error state $\tilde{\theta}$ and its derivative $\tilde{\theta}'$. Methodologies like polynomial interpolation and kernel-based nonparametric regression can be used to approximate Term A. In this work, approximation based on Taylor's series is used. Particularly, the two-dimensional Taylor series expansion of function h about the target states $\bar{\theta}$ and $\bar{\theta}'$ is approximated up to n^{th} order. The choice of n can depend on the error states $\tilde{\theta}$ and $\tilde{\theta}'$ and the effect of bootstrap current on plasma dynamics in a given tokamak scenario. Suppose $g : (\hat{\rho}, \tilde{\theta}, \tilde{\theta}', t) \mapsto g(\hat{\rho}, \tilde{\theta}, \tilde{\theta}', t)$ represents the bootstrap error function, i.e., the approximation of Term A. The final error model takes the form

$$\dot{\tilde{\theta}} = \left[F\left[\ G\tilde{\theta}\ \right]'\right]' + \left[H\tilde{j}_{aux}\right]' + g. \tag{11}$$

3. CONTROL SYNTHESIS

3.1 Lyapunov-based Control Design and Stability Analysis

In this work, Lyapunov analysis is used to prove the exponential convergence of the error state $\tilde{\theta}$ to the origin. Before defining a Lyapunov function, we assume a strictly positive continuous function $f : \hat{\rho} \mapsto [\epsilon, \infty)$ ($\epsilon > 0$) exists in the Sobolev space $W^{2,2}([0, 1])$ such that

$$f''FG + f'\left[FG' + (FG)'\right] - f(FG')' \leq -\alpha f, \tag{12}$$

where α is a positive scalar. Note that $W^{2,2}([0, 1])$ is the space of functions on $[0, 1]$ such that their weak derivatives up to the 2^{nd} order have a finite L^2 norm (Adams and Fournier, 2003). The existence of f satisfying (12) is critical for proving the stability result; however, as shown below, it does not appear in the control law. Now, define the Lyapunov function $V : \tilde{\theta} \in L^2 \mapsto V(\tilde{\theta}) \in \mathbb{R}$ as

$$V(\tilde{\theta}) := \frac{1}{2} \int_0^1 f(\hat{\rho}) \tilde{\theta}(\hat{\rho})^2 d\hat{\rho}. \tag{13}$$

Since the function f is positive, the above Lyapunov function can be used to define a weighted norm as $\|\tilde{\theta}\|_f = \sqrt{V(\tilde{\theta})}$ (even if f does not satisfy (12)). Since the positive function f is continuous on a compact domain, it is bounded from above and below by a positive constant. This fact can be used to prove that the weighted norm $\|\cdot\|_f$ is equivalent to the L^2 norm, which implies that the convergence in the weighted norm is equivalent to the convergence in the L^2 norm. In the following analysis, Lyapunov theory is used to prove that the error state $\tilde{\theta}$ converges exponentially to the origin in the weighted norm sense.

Theorem 1. The time derivative of the Lyapunov function defined in (13) satisfies the inequality

$$\dot{V} \leq -\alpha V(\tilde{\theta}) + \int_0^1 f\tilde{\theta}\left(H\tilde{j}_{aux}\right)' d\hat{\rho} + \underbrace{\int_0^1 f\tilde{\theta} g d\hat{\rho}}_{\text{B}}. \quad (14)$$

Proof. The proof follows the steps involved in traditional Lyapunov analysis. The time derivative of the Lyapunov function defined in (13) is given by $\dot{V} = \int_0^1 f(\hat{\rho})\tilde{\theta}\dot{\tilde{\theta}}d\hat{\rho}$. Expanding (11) and substituting the resulting expression for $\dot{\tilde{\theta}}$ in the above equation gives us

$$\dot{V} = \int_0^1 f\tilde{\theta}\Big[(FG')'\tilde{\theta} + [FG' + (FG)']\,\tilde{\theta}' + FG\tilde{\theta}'' + \left(H\tilde{j}_{aux}\right)' + g\Big] d\hat{\rho}. \quad (15)$$

Using integration by parts and simplifying the resulting equation gives us

$$\dot{V} = \frac{1}{2}\int_0^1 [f''FG + f'\,[FG' + (FG)'] - f(FG')']\,\tilde{\theta}^2 d\hat{\rho} + \int_0^1 f\tilde{\theta}\left(\left(H\tilde{j}_{aux}\right)' + g\right) d\hat{\rho} - \underbrace{\int_0^1 fFG\tilde{\theta}'^2 d\hat{\rho}}_{\text{Term C}\geq 0}. \quad (16)$$

Since f is chosen such that the inequality in (12) holds and Term C in the above equation is always nonnegative, the time derivative of the Lyapunov function is bounded from above by

$$\dot{V} \leq -\frac{1}{2}\int_0^1 f\tilde{\theta}^2 d\hat{\rho} + \int_0^1 f\tilde{\theta}\left(\left(H\tilde{j}_{aux}\right)' + g\right) d\hat{\rho}, \quad (17)$$

which gives the desired inequality.

A similar inequality for the linear (i.e., $g = 0$) normalized version of the model given in (11) is shown in Argomedo et al. (2013b). In the linear case, it can be shown that the system stabilizes to the origin even in the absence of the input $\tilde{j}_{aux}$. This is evident when g and $\tilde{j}_{aux}$ in (11) are set to 0. The above inequality simplifies to $\dot{V} \leq -\alpha V(\tilde{\theta})$. From Lyapunov theorem (Walker, 2013), we conclude that $\|\tilde{\theta}(\cdot,t)\|_f \leq e^{-\frac{\alpha}{2}t}\|\tilde{\theta}(\cdot,0)\|_f$. Note that even though an input is not required in this case, a carefully selected input $\tilde{j}_{aux}$ can increase the rate of convergence. For instance, by selecting $\tilde{j}_{aux}$ as

$$\tilde{j}_{aux} = -\frac{1}{H}\int_0^{\hat{\rho}} \frac{\beta}{2}\tilde{\theta} d\breve{\rho}, \quad (18)$$

it is possible to show that $\|\tilde{\theta}(\cdot,t)\|_f \leq e^{-\frac{\alpha+\beta}{2}t}\|\tilde{\theta}(\cdot,0)\|_f$. The above analysis is not longer valid in the nonlinear case (i.e., when $g \neq 0$) because the presence of nonlinear bootstrap error term g in the model given in (11) introduces Term B in the inequality given in (14). Thus, if $\tilde{j}_{aux} = 0$, the error state $\tilde{\theta}$ may not converge to the origin (unlike the linear case discussed above). An input is necessary to compensate for the effect of the nonlinear bootstrap term and ensure convergence.

Theorem 2. If the term $\tilde{j}_{aux}$ is chosen as

$$\tilde{j}_{aux} = -\frac{1}{H}\int_0^{\hat{\rho}} \left(\frac{\beta}{2}\tilde{\theta} + g\right) d\breve{\rho}, \quad (19)$$

where $\beta \geq 0$ is a scalar constant, then the equilibrium at the origin is exponentially stable.

Proof. The proof follows from the inequality given in Theorem 1. Substituting (19) into (14) results in the inequality

$$\dot{V} \leq -\int_0^1 \beta\frac{1}{2}f\tilde{\theta}^2 d\hat{\rho} - \alpha\frac{1}{2}\int_0^1 f\tilde{\theta}^2 d\hat{\rho} = -(\alpha+\beta)V. \quad (20)$$

Using Lyapunov theorem (Walker, 2013), we get the inequality $\|\tilde{\theta}(\cdot,t)\|_f \leq e^{-\frac{(\alpha+\beta)}{2}t}\|\tilde{\theta}(\cdot,0)\|_f$. which proves the theorem.

Note that the input given by (19) stabilizes the system by canceling the nonlinear term g in (11). Recall that the term g is the error between the plant and target system's bootstrap terms. Thus, in other words, the input regulates the bootstrap current of the plant to match the corresponding value of the target plant to get the desired stabilization. The term $(\beta/2)\tilde{\theta}$ in (19) is included to increase the rate of convergence of the error state $\tilde{\theta}$.

3.2 Physical Inputs Computation

The total auxiliary source profile j_{aux} is given by

$$j_{aux}(\hat{\rho},t) = \underbrace{-\frac{1}{H}\int_0^{\hat{\rho}} \left(\frac{\beta}{2}\tilde{\theta} + g\right) d\breve{\rho}}_{\tilde{j}_{aux}(\hat{\rho},t)} + \bar{j}_{aux}(\hat{\rho},t). \quad (21)$$

In any given tokamak scenario, the auxiliary current is driven by actuators like NBIs and EC H&CDs. The plasma control system can prescribe the power of these actuators. Thus, it is necessary to calculate the auxiliary drive power values from the virtual input in (21). To make computation feasible, the infinite-dimensional control law in (21) is first approximated using a finite-difference scheme. Consider N finite-difference nodes at $\hat{\rho}_1,\ldots,\hat{\rho}_N$. The assumption is that none of these nodes coincide with the boundary since the boundary conditions are fixed. Then the approximated control input vector is

$$\boldsymbol{j_{aux}} = [j_{aux,1},\ldots,j_{aux,N}]^T, \quad (22)$$

where $j_{aux,i}(t) = j_{aux}(\hat{\rho}_i,t)$. The relation between the control input vector $\boldsymbol{j_{aux}}$ and the auxiliary powers is modeled using the control-oriented models developed in Barton et al. (2013). Suppose there are m and n actuators available for safety factor profile control. The control-oriented model for i^{th} component of the vector $j_{aux,i}$ is given by

$$j_{aux,i}(t) = \sum_{j=1}^{m} g_{nb,j,i}u_{nb,j}(t) + \sum_{k=1}^{n} g_{ec,k,i}u_{ec,k}(t), \quad (23)$$

where $g_{nb,j,i} = g_{nb,j}(\hat{\rho}_i)$, $g_{ec,k,i} = g_{ec,k}(\hat{\rho}_i)$. Here, the terms $g_{nb,j}$ and $g_{ec,k}$ are profiles that account for the current depositions of j^{th} NBI and k^{th} EC H&CD, respectively. The terms $u_{nb,j}$ and $u_{ec,k}$ in (23) are defined as

$$u_{nb,j} := I_p^{\gamma(\lambda_{nb}-\frac{3}{2})}P_{tot}^{\epsilon(\lambda_{nb}-\frac{3}{2})}\bar{n}_e^{\zeta(\lambda_{nb}-\frac{3}{2})-1}P_{nb,j} \quad (24)$$

$$u_{ec,k} := I_p^{\gamma(\lambda_{ec}-\frac{3}{2})}P_{tot}^{\epsilon(\lambda_{ec}-\frac{3}{2})}\bar{n}_e^{\zeta(\lambda_{ec}-\frac{3}{2})-1}P_{ec,k}. \quad (25)$$

In (24), (25), the terms $P_{nb,j}$ and $P_{ec,k}$ are j^{th} NBI and k^{th} EC H&CD powers, respectively, λ_{nb} and λ_{ec} are constants that accounts for NBI and EC H&CD current-drive efficiencies, respectively. Note that the total power P_{tot} is related to the NBI and EC H&CD powers through the equation

$$P_{tot} = \sum_{j=1}^{m} P_{nb,j} + \sum_{k=1}^{n} P_{ec,k} + \sum_{l=1}^{n_o} P_{o,l}, \qquad (26)$$

where n_o is the number of additional actuators that are tuned to heat the plasma (without driving the net current), and P_l is the power of l^{th} additional actuator. Once the values of P_{tot}, $P_{nb,l}$ and $P_{ec,k}$ are prescribed the corresponding controllers, the values of $P_{o,l}$ are chosen such that (26) is satisfied. Thus, the relation between the control input vector $\boldsymbol{j}_{aux}$ and the auxiliary powers is given by the equation

$$\boldsymbol{j_{aux}}(t) = G^*(t)\boldsymbol{P}_{aux}(t), \qquad (27)$$

where

$$\boldsymbol{P}_{aux} = [P_{nb,1}, \ldots, P_{nb,m}, P_{ec,1}, \ldots, P_{ec,n}]^T, \qquad (28)$$

$$G^* = [G^*_{nbi}, G^*_{ec}], \qquad (29)$$

$$G^*_{nb} = G_{nb} \times I_p^{\gamma(\lambda_{nb}-\frac{3}{2})} P_{tot}^{\epsilon(\lambda_{nb}-\frac{3}{2})} \bar{n}_e^{\zeta(\lambda_{nb}-\frac{3}{2})-1}, \qquad (30)$$

$$G^*_{ec} = G_{ec} \times I_p^{\gamma(\lambda_{ec}-\frac{3}{2})} P_{tot}^{\epsilon(\lambda_{ec}-\frac{3}{2})} \bar{n}_e^{\zeta(\lambda_{ec}-\frac{3}{2})-1}, \qquad (31)$$

$$G_{nb} = \begin{bmatrix} \boldsymbol{g}_{nb,1} \\ \cdots \\ \boldsymbol{g}_{nb,N} \end{bmatrix}, G_{ec} = \begin{bmatrix} \boldsymbol{g}_{ec,1} \\ \cdots \\ \boldsymbol{g}_{ec,N} \end{bmatrix}, \qquad (32)$$

$$\boldsymbol{g}_{nb,i} = [g_{nb,1,i}, \ldots, g_{nb,m,i}], \qquad (33)$$

$$\boldsymbol{g}_{ec,k} = [g_{ec,1,k}, \ldots, g_{ec,n,k}]. \qquad (34)$$

Thus, at any given time t, the auxiliary powers (elements of $\boldsymbol{P}_{aux}$ vector) can be computed from the virtual input vector $\boldsymbol{j_{aux}}$ by solving the linear equation (27). In any given tokamak scenario, the number of actuators available for safety factor control is limited. On the other hand, the number of finite-difference nodes must be chosen sufficiently high so that the approximated control inputs is close to the infinite-dimensional control input. Thus, the system given in (27) is overdetermined for most tokamak scenarios. In such cases, a solution may not exist. Least squares minimization can be used to determine the best possible combination of auxiliary powers that create an input profile closest to the one generated by (21).

Remark: Model uncertainties and controller errors can cause the controller to deviate from ideal performance. The uncertainties in the model can arise from any unaccounted plasma dynamics or the bootstrap approximation error. On the other hand, controller errors can arise from the introduction of finite-difference approximation and the residual from solving the least squares problem as discussed above.

4. NUMERICAL SIMULATIONS

The proposed control algorithm was tested using nonlinear simulations for a DIII-D tokamak scenario. The DIII-D configuration used in shot 147634 was used during the simulations. The plant model, obtained by approximating (5) using the finite-difference scheme, was simulated by considering 41 equidistant finite-difference nodes. In the simulations, 0.5D control-oriented models for electron temperature T_e and plasma resistivity η, first introduced in Barton et al. (2013), were used. Readers can refer to Pajares and Schuster (2021) for the steps involved in deriving the finite-dimensional control-oriented plant model based on empirical laws. On the other hand, the finite-difference scheme for the controller considered 19 equidistant control nodes at $\hat{\rho} = 0.05, \ldots, 0.95$. In other words, the control input vector $\boldsymbol{j}_{aux}(t)$ has 19 elements, which are computed by evaluating the infinite-dimensional control law (21) at each of the control nodes. A total of three auxiliary drives (1 on-axis co-current NBI, 1 off-axis co-current NBI, 1 EC H&CD cluster) were assumed to be available for safety factor control. Furthermore, one additional EC H&CD was assumed to be available to account for the discrepancy between the total power and the sum of auxiliary drive powers, i.e., the term n_o in (26) is equal to 1. The saturation limits of the NBIs and EC H&CD were assumed to be 8 MW and 4 MW, respectively. The scalar constant β in (21) was selected as $\beta = 2\times10^{-8}$. The controller was activated at 3 seconds.

In the simulations, open-loop (FF only) and closed-loop (FF+FB) cases were considered. The open-loop case was designed to replicate a scenario where the state drifts from the target during the flat-top phase. Such drifting can occur in the presence of model uncertainties or the accumulation of errors. The goal of the closed-loop case was to check if the controller could maintain approximately zero error. Figure 2 shows the results obtained in the open-loop and closed-loop simulations. The figure shows the poloidal flux gradient profile $\theta(\cdot, t)$ at $t = 6$ seconds for $\hat{\rho} \in [0.05, 0.95]$ since the maximum discrepancy between the target and the open-loop profile was observed in this region. The poloidal flux gradient profile obtained in the closed-loop case matches the given target. The figure also shows the evolution of the poloidal flux gradient values at $\hat{\rho} = 0.4$ and $\hat{\rho} = 0.6$. Clearly, the poloidal flux gradient drifting is not observed in the closed-loop case. Figure 3 shows the auxiliary powers in both the open-loop and closed-loop cases. As discussed above, the auxiliary powers in the closed-loop case were obtained by solving a least squares optimization problem with the cost function $\|\boldsymbol{j}_{aux} - G^*(t)\boldsymbol{P}_{aux}(t)\|_2^2$. In the cost function, the terms $\boldsymbol{P}_{aux}(t)$, $G^*(t)$ are defined in (28) and (29), respectively. The vector $\boldsymbol{j}_{aux}$ is computed from (21), (22) and (23). Figure 3 also shows the total power P_{tot} used in the simulations. Since the sum of auxiliary powers $\sum \boldsymbol{P}_{aux}$ is not equal to the total power, the power of the additional heating actuator $P_{o,1}$ (also shown in Figure 3) is modulated to satisfy (26).

5. CONCLUSION

This work develops a nonlinear Lyapunov-based distributed control law to regulate the safety factor profile in tokamak scenarios associated with high-bootstrap current fraction. The infinite-dimensional controller is designed to account for the nonlinear effects of bootstrap current on the safety factor dynamics. Stability analysis shows that the L_2 norm of the system error converges exponentially to zero. The analysis also shows that convergence might not be possible when the nonlinear effects of the bootstrap current are pronounced. A detailed discussion of the steps involved in computing the auxiliary drive powers from the virtual infinite-dimensional control law is presented. The effect of model uncertainties and controller errors on the system performance is also discussed in detail. Nonlinear DIII-D tokamak scenario simulations show that the controller effectively tracks a given target. Future extensions of the work can include developing a robust version of the proposed controller, integrating a function estimator with the controller to estimate model uncertainties, and testing the effectiveness of the proposed controller in experiments.

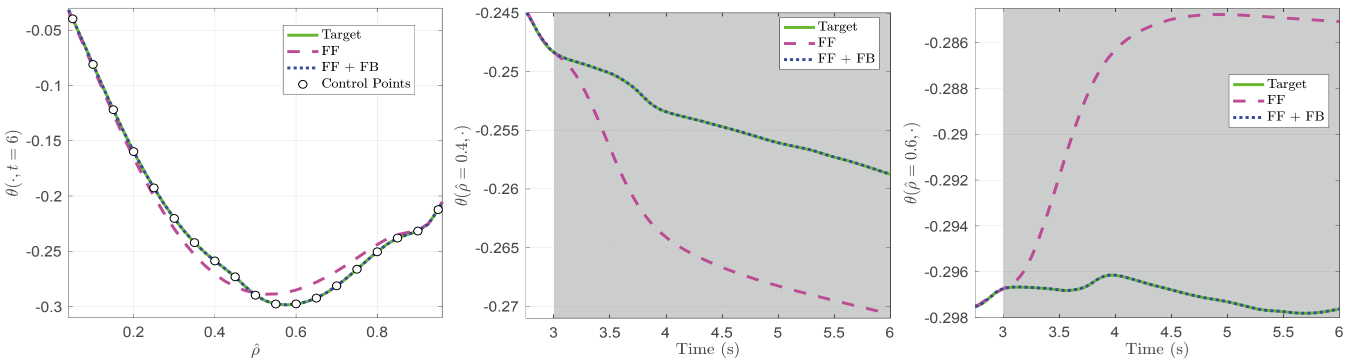

Fig. 2. Poloidal flux gradient - $\theta(\cdot, t = 6)$ (left), $\theta(\hat{\rho} = 0.4, \cdot)$ (center), $\theta(\hat{\rho} = 0.6, \cdot)$ (right)

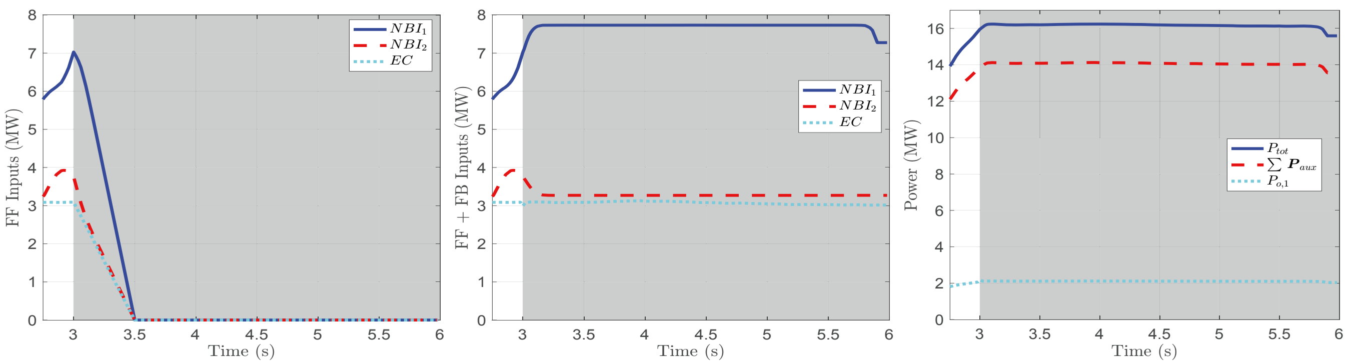

Fig. 3. Input powers: feedforward - FF (left), feedforward + feedback - FF+FB (center), total & heating actuator (right)

REFERENCES

Adams, R.A. and Fournier, J.J. (2003). *Sobolev spaces*. Elsevier.

Argomedo, F.B. et al. (2013a). A Strict Control Lyapunov Function for a Diffusion Equation With Time-Varying Distributed Coefficients. *IEEE Transactions on Automatic Control*, 58(2), 290–303. doi: 10.1109/TAC.2012.2209260.

Argomedo, F.B. et al. (2013b). Lyapunov-based distributed control of the safety-factor profile in a tokamak plasma. *Nuclear Fusion*, 53(3). doi:10.1088/0029-5515/53/3/033005.

Barton, J.E. et al. (2013). Physics-based control-oriented modeling of the safety factor profile dynamics in high performance tokamak plasmas. In *52nd IEEE Conference on Decision and Control*, 4182–4187. doi: 10.1109/CDC.2013.6760531.

Barton, J. et al. (2015). Physics-model-based nonlinear actuator trajectory optimization and safety factor profile feedback control for advanced scenario development in DIII-D. *Nuclear Fusion*, 55(9). doi:10.1088/0029-5515/55/9/093005.

Boyer, M. et al. (2015). Central safety factor and β_n control on NSTX-U via beam power and plasma boundary shape modification, using TRANSP for closed loop simulations. *Nuclear Fusion*, 55(5), 053033. doi: 10.1088/0029-5515/55/5/053033.

Hinton, F.L. and Hazeltine, R.D. (1976). Theory of plasma transport in toroidal confinement systems. *Reviews of Modern Physics*, 48(2), 239–308. doi: 10.1103/RevModPhys.48.239.

Mavkov, B. et al. (2018). Experimental validation of a Lyapunov-based controller for the plasma safety factor and plasma pressure in the TCV tokamak. *Nuclear Fusion*, 58(5), 056011. doi:10.1088/1741-4326/aab16a.

Morosohk, S. et al. (2022). Estimation of the electron temperature profile in tokamaks using analytical and neural network models. In *American Control Conference (ACC)*.

Ou, Y. et al. (2011). Receding-horizon optimal control of the current profile evolution during the ramp-up phase of a tokamak discharge. *Control Engineering Practice*, 19(1), 22–31. doi:10.1016/j.conengprac.2010.08.006.

Pajares, A. and Schuster, E. (2016). Safety factor profile control in tokamaks via feedback linearization. In *2016 IEEE 55th Conference on Decision and Control (CDC)*. doi:10.1109/CDC.2016.7799140.

Pajares, A. and Schuster, E. (2021). Current profile and normalized beta control via feedback linearization and Lyapunov techniques. *Nucl. Fusion*, 21.

Paruchuri, S.T. et al. (2021). Minimum safety factor control in tokamaks via optimal allocation of spatially moving electron cyclotron current drive. In *60th IEEE Conference on Decision and Control*.

Sauter, O. et al. (1999). Neoclassical conductivity and bootstrap current formulas for general axisymmetric equilibria and arbitrary collisionality regime. *Physics of Plasmas*, 6(7), 2834–2839. doi:10.1063/1.873240.

Walker, J.A. (2013). *Dynamical systems and evolution equations: theory and applications*, volume 20. Springer Science & Business Media.

Wehner, W. et al. (2017). Optimal current profile control for enhanced repeatability of L-mode and H-mode discharges in DIII-D. *Fusion Engineering and Design*, 123, 513–517. doi:10.1016/j.fusengdes.2017.03.022.

Wesson, J. and Campbell, D.J. (2011). *Tokamaks*, volume 149. Oxford university press.